A General Numerical Method for Analyzing the Linear Stability of Stratified Parallel Shear Flows

Tim Rees & Adam Monahan

July 2014

A General Numerical Method for Analyzing the Linear Stability of Stratified Parallel Shear Flows

TIM REES AND ADAM MONAHAN

School of Earth and Ocean Sciences, University of Victoria, Victoria, British Columbia, Canada

(Manuscript received 3 February 2014, in final form 23 July 2014)

ABSTRACT

The stability analysis of stratified parallel shear flows is fundamental to investigations of the onset of turbulence in atmospheric and oceanic datasets. The stability analysis is performed by considering the behavior of small-amplitude waves, which is governed by the Taylor–Goldstein (TG) equation. The TG equation is a singular second-order eigenvalue problem, whose solutions, for all but the simplest background stratification and shear profiles, must be computed numerically. Accurate numerical solutions require that particular care be taken in the vicinity of critical layers resulting from the singular nature of the equation. Here a numerical method is presented for finding unstable modes of the TG equation, which calculates eigenvalues by combining numerical solutions with analytical approximations across critical layers. The accuracy of this method is assessed by comparison to the small number of stratification and shear profiles for which analytical solutions exist. New stability results from perturbations to some of these profiles are also obtained.

1. Introduction

The complexity of processes and range of scales in fully nonlinear geophysical flows poses a significant barrier in the understanding of their dynamics. Appropriately constructed idealized linear models can reduce the complexity and reveal valuable insights into the behavior of a flow. However, even with strong simplifying assumptions, the mathematical problems that remain are often substantial and require careful treatment. Such is the case for the problem of calculating linearly unstable wave solutions for stratified parallel shear flows. This problem has important applications in the geophysical setting (Drazin and Reid 1981), and it is of particular relevance in analyzing observations of the onset of turbulence in the atmospheric and oceanic boundary layer (e.g., De Baas and Driedonks 1985; Sun et al. 1998). As we shall see, the wave stability problem is particularly difficult because the combination of stratification and shear leads to a singular eigenvalue problem (the unstratified shear problem is also singular, but to a lesser degree). In this paper we describe a new numerical method for the calculation of these unstable waves.

In the small-amplitude limit, the Taylor–Goldstein (TG) equation models the balance between the destabilizing effects of shear and the (generally) stabilizing effects of stratification for an inviscid Boussinesq fluid. Here we adopt a dimensionless form of the TG equation in two spatial coordinates. Squire's theorem (Drazin and Reid 1981) justifies the reduction to two spatial coordinates, and the task of analyzing a three-dimensional flow can be treated as a collection of two-dimensional problems (e.g., De Baas and Driedonks 1985). The nondimensionalization is carried out as follows. Using tildes to denote dimensional variables, we introduce dimensionless coordinates $(x, z) = (\tilde{x}/h, \tilde{z}/h)$, where x is the horizontal coordinate, z is the vertical coordinate, and h is a characteristic length scale. We suppose the background velocity is of the form $[\tilde{U}(\tilde{z}), 0]$ and write $\tilde{U}(\tilde{z}) = VU(z)$, where V is a characteristic speed scale and $U(z)$ is the dimensionless velocity profile. We write the squared buoyancy frequency as $\tilde{N}^2(\tilde{z}) = -(g/\rho_0)(d\overline{\rho}/d\tilde{z})$, where g is the gravitational constant, and the background density $\tilde{\rho}(\tilde{z}) = \rho_0 + \overline{\rho}(\tilde{z})$ is split into a constant value and a vertically varying component. Letting σ denote a typical value of $\overline{\rho}/\rho_0$, we define the bulk Richardson number $J = \sigma gh/V^2$ and the

Corresponding author address: Tim Rees, School of Earth and Ocean Sciences, University of Victoria, P.O. Box 3065 STN CSC, Victoria BC V8W 3V6, Canada.
E-mail: timothy.rees@gmail.com

DOI: 10.1175/JTECH-D-14-00034.1

dimensionless squared buoyancy frequency via $N^2(z) = (h^2/JV^2)\tilde{N}^2(\tilde{z})$.

With these conventions, a horizontally propagating plane wave with streamfunction of the form $\psi(x, z, t) = \mathrm{Re}\{\phi(z)\exp[i\alpha(x - ct)]\}$ satisfies the TG equation, defined as

$$\phi''(z) + \left\{\frac{JN^2(z)}{[U(z) - c]^2} - \frac{U''(z)}{U(z) - c} - \alpha^2\right\}\phi(z) = 0. \quad (1)$$

The dimensionless wavenumber and phase speed are denoted by α and c, respectively. The bulk Richardson number J serves as a convenient control of the strength of the stratification. An important special case of the TG equation, known as the Rayleigh equation, arises in the unstratified limit $J = 0$.

With appropriate boundary conditions (discussed further in section 2), the TG equation is an eigenvalue problem for c with corresponding eigenfunction $\phi(z)$. The eigenvalues $c = c_r + ic_i$ may be real or complex, and if there exists a solution with $c_i > 0$, then the flow is said to be unstable. Finding the unstable modes of a given flow profile, if there are any, is usually the primary motivation for studying the TG equation and is the sole focus of our numerical method. The unstable modes are of great significance because they grow exponentially in time as $\exp(\alpha c_i t)$ by extracting energy from the background shear profile. The growth of the unstable modes will quickly lead to a violation of the small-amplitude assumption used in the derivation of the TG equation. As a result, the TG equation does not serve as a model for the temporal evolution of unstable waves, merely as a means of predicting their presence and initial growth characteristics.

Since its independent derivations by Taylor (1931) and Goldstein (1931), the TG equation has been used in a range of theoretical, experimental, and numerical investigations. Examples include the numerous analytical studies discussed by Drazin and Reid (1981); a numerical investigation of several idealized but important shear profiles (Hazel 1972); observations and analysis of shear instabilities in the atmospheric boundary layer (e.g., De Baas and Driedonks 1985); the ocean (e.g., Sun et al. 1998; Smyth et al. 2011), and estuarine flows (e.g., Tedford et al. 2009); and distinguishing Kelvin–Helmholtz waves from Holmboe waves (Carpenter et al. 2010). In addition, slightly modified forms of the TG equation have been used in numerical studies of atmospheric wave generation by shear (Lalas and Einaudi 1976; Mastrantonio et al. 1976; Mobbs and Darby 1989). However, with the notable exceptions of Hazel (1972) and Mobbs and Darby (1989), few details on the actual implementation of a numerical method for the inviscid TG equation can be found. Here we attempt to fill that gap by describing a numerical method for the TG equation. Our method, referred to as "TGsolver" and implemented in MATLAB, is designed for the task of calculating the unstable modes of a given shear and stratification profile.

Two well-known analytical results play an important role in our numerical approach: the Richardson number criterion and Howard's semicircle theorem [derivations of both of these results are presented in Kundu and Cohen (2004)]. The Richardson number criterion states that if the flow is linearly unstable, then the local Richardson number, defined by $\mathrm{Ri}(z) = JN^2(z)/(dU/dz)^2$, must satisfy

$$\min_z \mathrm{Ri}(z) < \frac{1}{4} \quad (2)$$

somewhere in the flow. Condition (2) is a necessary condition for instability and thus can be used to classify broad regions within the parameter space as stable. This condition also confirms the intuitive notion that sufficiently strong stratification always has a stabilizing influence on a flow. Howard's semicircle theorem states that for any unstable eigenvalue $c = c_r + ic_i$, the real and imaginary components must satisfy

$$\left(c_r - \frac{U_{\max} + U_{\min}}{2}\right)^2 + c_i^2 \le \left(\frac{U_{\max} - U_{\min}}{2}\right)^2. \quad (3)$$

This condition has two very important consequences in the present setting. First, it confines the search for eigenvalues to a well-defined region in the (c_r, c_i) plane. Second, condition (3) suggests that for any unstable mode with small c_i, we can expect the TG equation to exhibit singular behavior. This follows because c_r must lie within the range of $U(z)$ and thus $[U(z) - c]^2$ may take on very small values within the computational domain.

Any point z_c where $U(z_c) - c_r = 0$ is referred to as a critical point. The small neighborhood around such a point, where the large values of $JN^2(z)/[U(z) - c]^2$ and $U''(z)/[U(z) - c]$ provide the dominant influence on the behavior of $\phi(z)$, is referred to as a critical layer. It is the behavior of solutions within critical layers that make the TG equation a challenge to solve numerically. The singular behavior of an eigenfunction within a critical layer is not physical, but arises from the neglect of viscosity, density (heat) diffusion, and nonlinearity in the equations of motion (see Maslowe 1986 for a discussion). As demonstrated by Smyth et al. (2011), including viscous and diffusive effects in a numerical model is a viable option, but it leads to higher-order equations. In our approach to the TG equation, we treat the singular

behavior by approximating eigenfunctions with series expansions across critical layers.

In what follows, we describe our numerical method and illustrate its use on several idealized problems. In section 2 we describe the details of the numerical method and present our treatment of critical layers. In section 3 the method is illustrated on several example problems and compared with existing results where possible. A discussion is given in section 4, and conclusions are drawn in section 5. Finally, appendices are included with details of the series expansions of solutions in the critical layers and notes on the MATLAB implementation.

2. The numerical method

The direct approach to finding eigenvalues of Eq. (1) would be to multiply through by $(U - c)^2$, write the TG equation as a polynomial eigenvalue problem, discretize, and then solve as a generalized matrix eigenvalue problem. The polynomial eigenvalue problem takes the form

$$c^2 M_2 \phi + c M_1 \phi + M_0 \phi = 0, \tag{4}$$

where the operators M_0, M_1, M_2 are defined by $M_2 = d^2/dz^2 - \alpha^2$, $M_1 = -2U d^2/dz^2 + U'' + 2\alpha^2 U$, and $M_0 = U^2 d^2/dz^2 + JN^2(z) - U''U - \alpha^2 U^2$, respectively. The discretization step would be to approximate these operators on a set of grid points using matrices. However, Howard's semicircle theorem suggests that this approach is generally doomed to failure. This failure follows because, for any unstable mode, we have c_r in the range of $U(z)$ and the magnitude of c_i is not known a priori. It is therefore not possible, in general, to select a discretization capable of resolving critical layers. In addition, as we shall see shortly, the application of numerical radiation boundary conditions involves a nonlinear function of c that cannot be implemented with the direct approach.

A shooting method is a natural choice for the TG equation, as it reduces the eigenvalue problem to one of optimization and thus allows for control over the search region in the (c_r, c_i) plane. As we shall discuss, the shooting process also facilitates the task of imposing the relevant boundary conditions, even in the radiating case. Shooting methods are a popular choice for solving boundary value problems in general and are described extensively by Ascher et al. (1988). Hazel (1972) used a shooting method in his analysis of solutions to the TG equation for idealized flows and stratification profiles. The numerical method that follows is inspired by this earlier work.

For the remainder of this section we will assume α and J are given and fixed; finding unstable solutions throughout the (α, J) plane is achieved by iterating over the desired values.

a. The shooting method

We define the computational domain to be the interval $-H \le z \le H$. This interval is split into two subdomains about a matching point z_m. Typically we set $z_m = 0$; however, if a critical layer approximation is required, this value is modified (as discussed further in section 2d). We use the subscript "$\mathcal{B}$" when referring to the bottom (lower) subdomain $-H \le z \le z_m$, and "$\mathcal{T}$" when referring to the top (upper) subdomain $z_m \le z \le H$.

For a given value of $c = c_r + ic_i$, TGsolver evaluates an objective function $F(c_r, c_i)$ to determine how well the solutions on $\mathcal{B}$ and $\mathcal{T}$ match at z_m. The complex-valued objective function is defined by

$$F(c_r, c_i) = \det \begin{bmatrix} \phi_{\mathcal{B}}(z_m) & \phi_{\mathcal{T}}(z_m) \\ \phi'_{\mathcal{B}}(z_m) & \phi'_{\mathcal{T}}(z_m) \end{bmatrix}, \tag{5}$$

where primes indicate derivatives with respect to z. The pair (c_r, c_i) is a root of F if and only if the corresponding function

$$\phi(z) = \begin{cases} \phi_{\mathcal{T}}(z_m)\phi_{\mathcal{B}}(z) & \text{for} \quad z \in [-H, z_m], \\ \phi_{\mathcal{B}}(z_m)\phi_{\mathcal{T}}(z) & \text{for} \quad z \in [z_m, H], \end{cases} \tag{6}$$

is an eigenfunction of the original TG problem, assuming $\phi(z_m) \neq 0$ [the scaling factors $\phi_{\mathcal{T}}(z_m)$ and $\phi_{\mathcal{B}}(z_m)$ are chosen to ensure continuity across z_m]. Under these assumptions the roots of F correspond to eigenfunctions of the TG equation, and the problem is reduced to a root-finding problem for $F(c_r, c_i)$.

However, TGsolver does not search for roots of F directly. Instead, we define a cutoff value δ and solve the related optimization problem,

$$\min_{(c_r, c_i)} |F(c_r, c_i)|^2 \text{ subject to } c_i > \delta, \tag{7}$$

and accept any solutions for which the final objective is sufficiently small. The rationale behind this modification is that it allows us to retain control over the size of c_i values that arise, and thus the degree of singularity possible. A similar approach is employed by Mobbs and Darby (1989) to constrain c values away from the real axis.

Standard algorithms exist to solve the constrained optimization problem [Eq. (7)]; our implementation uses the MATLAB Optimization Toolbox (appendix A). To facilitate convergence to local minima, initial estimates

for c_r and c_i are required, and Howard's semicircle theorem [Eq. (3)] provides the necessary guidance. We simply construct a Cartesian grid over the semicircle in the complex c plane, and from each point compute a few iterations in the minimization of $|F(c_r, c_i)|^2$. Results are then sorted by objective value, and poorly converged solutions are discarded. The remaining iterates are clustered via k-means, and the cluster centers are used as seed points for the full minimization process, where many iterations are allowed. This procedure is intended to reduce computational cost by eliminating iterates that are unlikely to converge and focusing on those that are most likely to succeed.

b. Computing $\phi_{\mathcal{B}}(z)$ and $\phi_{\mathcal{T}}(z)$

The evaluation of $F(c_r, c_i)$ requires the calculation of $\phi_{\mathcal{B}}(z)$ and $\phi_{\mathcal{T}}(z)$ and their respective derivatives. In a traditional shooting method, this is achieved by using an initial-value problem (IVP) solver to step inward from the boundaries toward the matching point, and this approach was used by Hazel (1972). Our approach is to treat the problem on each subdomain as a separate boundary value problem (BVP) with an artificial boundary condition, discretize the linear TG operator, and solve the resulting matrix equation. The artificial boundary conditions we impose are

$$\phi_{\mathcal{B}}(z_m) = 1, \quad \phi_{\mathcal{T}}(z_m) = 1. \tag{8}$$

This has the drawback of preventing any eigenfunctions with roots exactly at z_m from being found, but such solutions could be recovered by repeating the calculation with the artificial condition

$$\phi'_{\mathcal{B}}(z_m) = 1, \quad \phi'_{\mathcal{T}}(z_m) = 1, \tag{9}$$

if desired.

In TGsolver we employ Chebyshev grids and differentiation matrices (taken from Trefethen 2000) on each subdomain. These powerful methods enable us to construct high-order approximations to functions and their derivatives with relatively few grid points. The discretization process reduces the TG equation to a linear system of algebraic equations on each subdomain. We will denote by $\hat{\boldsymbol{\phi}}_{\mathbf{B}}$ and $\hat{\boldsymbol{\phi}}_{\mathbf{T}}$ the approximations to $\phi_{\mathcal{B}}(z)$ and $\phi_{\mathcal{T}}(z)$, respectively, on the Chebyshev grid. Using an analogous definition on $\mathcal{T}$, we define the TG matrix operator on $\mathcal{B}$ by

$$\mathbf{L}_{\mathcal{B}} = \mathbf{D}^2 + \mathbf{A}, \tag{10}$$

where $\mathbf{D}$ is the Chebyshev differentiation matrix, and the jth diagonal entry in the diagonal matrix $\mathbf{A}$ is given by

$$\mathbf{A}_{jj} = \frac{JN^2(z_j)}{[U(z_j) - c]^2} - \frac{U''(z_j)}{U(z_j) - c} - \alpha^2, \tag{11}$$

where z_j is the jth Chebyshev grid point (with the index increasing as z decreases). Neglecting boundary conditions, the approximation of $\phi_{\mathcal{B}}(z)$ and $\phi_{\mathcal{T}}(z)$ is thus reduced to the solution of the following two matrix equations:

$$\mathbf{L}_{\mathcal{B}}\hat{\boldsymbol{\phi}}_{\mathbf{B}} = \hat{\mathbf{r}}_{\mathbf{B}}, \quad \mathbf{L}_{\mathcal{T}}\hat{\boldsymbol{\phi}}_{\mathbf{T}} = \hat{\mathbf{r}}_{\mathbf{T}}, \tag{12}$$

where all but the first and last entries of the right-hand sides $\hat{\mathbf{r}}_{\mathbf{B}}$ and $\hat{\mathbf{r}}_{\mathbf{T}}$ are zero. We now describe the modifications of $\mathbf{L}_{\mathcal{B},\mathcal{T}}$ and $\hat{\mathbf{r}}_{\mathbf{B},\mathbf{T}}$ that are necessary to apply the correct boundary conditions.

c. Boundary conditions

We must impose the artificial boundary conditions at z_m as well as physical boundary conditions at $z = \pm H$. The latter requires careful consideration, but the artificial conditions are imposed by simply setting

$$\begin{aligned} \mathbf{L}_{\mathcal{B}}(1, j) &= \delta_{1j}, \quad \hat{\mathbf{r}}_{\mathbf{B}}(1) = 1, \\ \mathbf{L}_{\mathcal{T}}(n, j) &= \delta_{nj}, \quad \hat{\mathbf{r}}_{\mathbf{T}}(n) = 1, \end{aligned} \tag{13}$$

where $\delta_{ij} = 1$ if $i = j$ and zero otherwise, and n is the number of points in the Chebyshev grid.

The two most physically relevant boundary conditions for the TG problem are rigid-lid and radiation conditions. Mixtures of these conditions (where one boundary is radiating, the other is rigid) are also relevant, but we will not discuss them in detail, as they can be implemented by combining the process for the radiation and rigid-lid conditions in an obvious manner.

For models of fluid confined between plane rigid boundaries at $z = \pm H$, eigenfunction solutions to the TG equation must satisfy $\phi(\pm H) = 0$. This ensures that no normal flow is present at the boundaries. These conditions are easily implemented by setting

$$\begin{aligned} \mathbf{L}_{\mathcal{B}}(n, j) &= \delta_{nj}, \quad \hat{\mathbf{r}}_{\mathbf{B}}(n) = 0, \\ \mathbf{L}_{\mathcal{T}}(1, j) &= \delta_{ij}, \quad \hat{\mathbf{r}}_{\mathbf{T}}(1) = 0. \end{aligned} \tag{14}$$

To approximate solutions for problems on unbounded domains, radiation conditions are necessary. To apply these conditions, we require additional constraints on the background velocity and stratification profiles. In particular, we require $N^2(z) \to$ constant and $U(z) \to$ constant as $|z| \to \infty$, though the constants need not be equal in the two directions. Letting $N^2_{\pm\infty}$ and $U_{\pm\infty}$ denote these constants as $z \to \pm\infty$, the far-field TG equation is approximated by

$$\phi''(z) - \gamma^2_{\pm}\,\phi(z) = 0 \quad \text{as} \quad z \to \pm\infty, \tag{15}$$

where

$$\gamma_{\pm}^2 = -\left[\frac{JN_{\pm\infty}^2}{(U_{\pm\infty}-c)^2} - \alpha^2\right]. \tag{16}$$

Since $\gamma_{\pm}$ will generally be complex, and the wave disturbance must decay in the far field, it follows that

$$\begin{aligned}\phi(z) &\sim B_- \exp\{\mathrm{sgn}[\mathrm{Re}(\gamma_-)]\gamma_- z\} \quad \text{as} \quad z \to -\infty,\\ \phi(z) &\sim B_+ \exp\{-\mathrm{sgn}[\mathrm{Re}(\gamma_+)]\gamma_+ z\} \quad \text{as} \quad z \to +\infty,\end{aligned} \tag{17}$$

where $B_{\pm}$ are constants and $\mathrm{sgn}[\mathrm{Re}(\gamma_{\pm})]$ denotes the sign of the real part of $\gamma_{\pm}$. The far-field relationships between ϕ and ϕ' follows from Eq. (17), and we apply these numerically by setting

$$\begin{aligned}\mathbf{L}_{\mathcal{B}}(n,j) &= \mathbf{D}(n,j) - \mathrm{sgn}[\mathrm{Re}(\gamma_-)]\gamma_-\delta_{nj}, \quad \hat{\mathbf{r}}_{\mathbf{B}}(n) = 0,\\ \mathbf{L}_{\mathcal{T}}(1,j) &= \mathbf{D}(1,j) + \mathrm{sgn}[\mathrm{Re}(\gamma_+)]\gamma_+\delta_{1j}, \quad \hat{\mathbf{r}}_{\mathbf{T}}(1) = 0\end{aligned} \tag{18}$$

for $1 \le j \le n$.

When applying radiation boundary conditions (BCs), it is apparent that the computational domain half-width H must be chosen large enough so that the velocity and stratification profiles are well approximated by their far-field values. The appropriate value of H does not depend on the wavenumbers under investigation; it is only necessary that H be large enough for the far-field relationship between ϕ and ϕ' to hold. It is also noteworthy that condition (18) depends on c in a nonlinear fashion. This poses no extra difficulty in the implementation of our shooting method, as the value of c is known prior to each calculation of $F(c_r, c_i)$.

d. *Treatment of critical layers*

Critical layers pose the primary difficulty in the numerical solution of the TG equation. The reason for this is evident in Fig. 1, where an eigenfunction with a critical layer at $z_c = 0$ is depicted. The cusplike structure of the real part of the eigenfunction and steep slope of the imaginary component within the critical layer can be explained from inspection of the asymptotic series expansions detailed in appendix B. For the simplest nondegenerate case, we see that the eigenfunction solution near a critical point z_c is, to leading order, a linear combination of the terms $(z - z_c - ic_i/U_c')^{r_1}$ and $(z - z_c - ic_i/U_c')^{r_2}$, where $0 < r_2 \le 1/2 \le r_1 < 1$. Differentiating these terms suggests that the eigenfunction will have a slope dominated by $(z - z_c - ic_i/U_c')^{r_2 - 1}$ near the critical point. When c_i/U_c' is small, the magnitude of this term grows rapidly as $z \to z_c$.

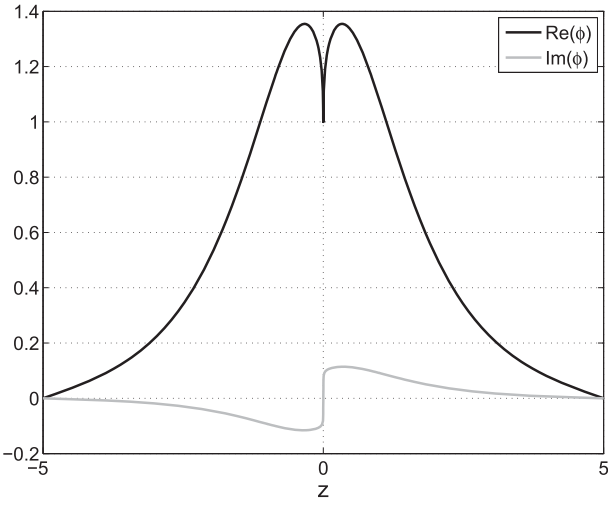

FIG. 1. The real and imaginary components of an eigenfunction with a critical layer approximation at $z_c = 0$. The cusplike structure of the real component and the very steep slope of the imaginary component of $\phi(z)$ are typical of critical layers.

The purpose of TGsolver is to find unstable eigenvalues ($c_i > 0$), and our casting of the eigenvalue problem as a constrained optimization problem largely allows us to avoid points for which the solution will be exactly singular. Even so, in certain parameter regimes the only unstable eigenvalues may have $|c_i/U_c'| \ll 1$, so that the eigenfunction is approximately singular near z_c.

To handle these troublesome points, we need a mechanism to decide when to use a critical layer approximation, and a method for determining the width of the critical layer. We accomplish the first task by using a slope threshold. For a candidate critical layer, we estimate the magnitude of the slope contributions at the critical point using the leading-order components of the series solutions (appendix B). If the sum of the slope contributions exceeds a preset cutoff value (which is a tunable parameter in TGsolver), then a critical layer approximation is used. The half-width of the critical layer, referred to as Δ_{cl}, is chosen so that $\Delta_{\mathrm{cl}} \ll |c_i/U_c'|$ (a heuristic condition that is based upon the derivation of the series approximations, as described in appendix B).

To apply the critical layer approximation, we adjust the size of the domains on which $\phi_{\mathcal{B}}$ and $\phi_{\mathcal{T}}$ are computed. Using the process described in the previous subsections, we solve for $\phi_{\mathcal{B}}(z)$ on the interval $-H \le z \le z_c - \Delta_{\mathrm{cl}}$ and for $\phi_{\mathcal{T}}(z)$ on the interval $z_c + \Delta_{\mathrm{cl}} \le z \le H$. With $\phi_1(z)$ and $\phi_2(z)$ linearly independent series solutions across the critical layer as defined in appendix B, we define the matrix

$$\mathbf{M}(z) = \begin{bmatrix}\phi_1(z) & \phi_2(z)\\ \phi_1'(z) & \phi_2'(z)\end{bmatrix} \tag{19}$$

and write the solution within the critical layer as

$$\begin{bmatrix} \phi_c(z) \\ \phi_c'(z) \end{bmatrix} = \mathbf{M}(z) \begin{pmatrix} a_1 \\ a_2 \end{pmatrix}, \tag{20}$$

where a_1 and a_2 are constants. By demanding continuity of any eigenfunction and its first derivative, and knowing the asymptotic form of the solution within the critical layer, Eq. (20) enables us to map the eigenfunction from one side of the critical layer to the other. By first computing an approximation of $\phi_{\mathcal{B}}(z - \Delta_{\rm cl})$, then $\phi_{\mathcal{B}}'(z - \Delta_{\rm cl})$, we can estimate

$$\begin{bmatrix} \phi_{\mathcal{B}}(z_c + \Delta_{\rm cl}) \\ \phi_{\mathcal{B}}'(z_c + \Delta_{\rm cl}) \end{bmatrix} = \mathbf{M}(z_c + \Delta_{\rm cl})\mathbf{M}^{-1}(z_c - \Delta_{\rm cl}) \begin{bmatrix} \phi_{\mathcal{B}}(z_c - \Delta_{\rm cl}) \\ \phi_{\mathcal{B}}'(z_c - \Delta_{\rm cl}) \end{bmatrix}. \tag{21}$$

With this matrix product, we have effectively integrated the solutions on $\mathcal{B}$ to the new matching point $z_m = z_c + \Delta_{\rm cl}$, and we evaluate the function $F(c_r, c_i)$ in Eq. (5) at this point.

The approach described above is limited to handling at most one critical layer. For nonmonotonic velocity profiles where multiple critical layers may be present at a value of c_r, it is necessary to set δ (the lower bound on c_i) to a relatively large value to ensure that the eigenfunctions are well behaved near any critical point. A future version of TGsolver will include expanded functionality for treating multiple critical layers.

3. Examples

We now present examples illustrating the use of TGsolver, providing comparisons with existing results where possible. We will pay particular attention to example profiles for which at least some analytical results are known.

a. *The Rayleigh problem of Michalke (1964)*

As a brief first example of TGsolver, we consider the following unstratified Rayleigh problem:

$$U(z) = \frac{1}{2}[1 + \tanh(z)], \quad N^2(z) = 0, \tag{22}$$

on an unbounded domain and attempt to reproduce some key results reported by Michalke (1964). It can be shown analytically that the unstable modes for this flow lie on the line $c_r = \frac{1}{2}$, and Michalke used this fact to simplify his calculations.

In TGsolver, we do not make use of this simplification, but as can be seen in Table 1, our calculations of c_i are in good agreement with Michalke's over a range of α values (although there is a very small positive bias of the TGsolver estimates). For each unstable eigenvalue reported in the table, we found $|c_r - 1/2| < 10^{-7}$.

TABLE 1. Comparison of TGsovler results with results from Michalke (1964, denoted as M64) for the Rayleigh problem [Eq. (22)]. Relative error is defined by $|c_i(\text{TGSolver}) - c_i(\text{M64})|/c_i(\text{M64})$.

α	c_i (TGsolver)	c_i (M64)	Relative error
0.1	0.4184	0.4184	4×10^{-4}
0.2	0.348 99	0.3487	7×10^{-4}
0.3	0.288 73	0.2885	1.0×10^{-3}
0.4	0.235 51	0.2352	1.2×10^{-3}
0.5	0.187 77	0.1875	1.4×10^{-3}
0.6	0.1444	0.1442	1.6×10^{-3}
0.7	0.104 52	0.1044	1.8×10^{-3}
0.8	0.067 481	0.0674	2.2×10^{-3}
0.9	0.032 778	0.0327	2.6×10^{-3}
1	0	0	0

b. *A mixing layer (Hazel 1972)*

We now consider a numerical problem investigated extensively by Hazel (1972). The velocity and stratification profile are given by

$$U(z) = \tanh(z), \quad N^2(z) = \operatorname{sech}^2(z). \tag{23}$$

The velocity and buoyancy profiles are plotted in Fig. 2. This flow represents a continuous model of a two-layer fluid and is special, as it is one of the few profiles for which analytical results are known. In particular, for an unbounded domain ($H \to \infty$) it can be shown (Drazin and Reid 1981) that the curve $J = \alpha(1 - \alpha)$ divides the first quadrant of the (α, J) plane into a stable and unstable region. At each point below the parabola, unstable solutions to the TG equation are present, and at each point above the parabola the flow is stable.

In Fig. 3 we plot contours of the imaginary part of the phase speed (logarithmically scaled) in the (α, J) plane, with the dashed line representing the known stability boundary. The calculations were performed with a radiating boundary condition at $H = 16$ to approximate an unbounded domain. All unstable modes are found to lie within the expected region in the (α, J) plane. This calculation extends Hazel's earlier results by also providing the phase speeds of the instabilities. The c_i values of unstable modes tend to increase with decreasing α and J, so that in the bottom left-hand part of the domain, the c_i values are large enough that critical layer approximations are unnecessary. As can be seen in the figure, however, c_i values are greatly reduced near the upper

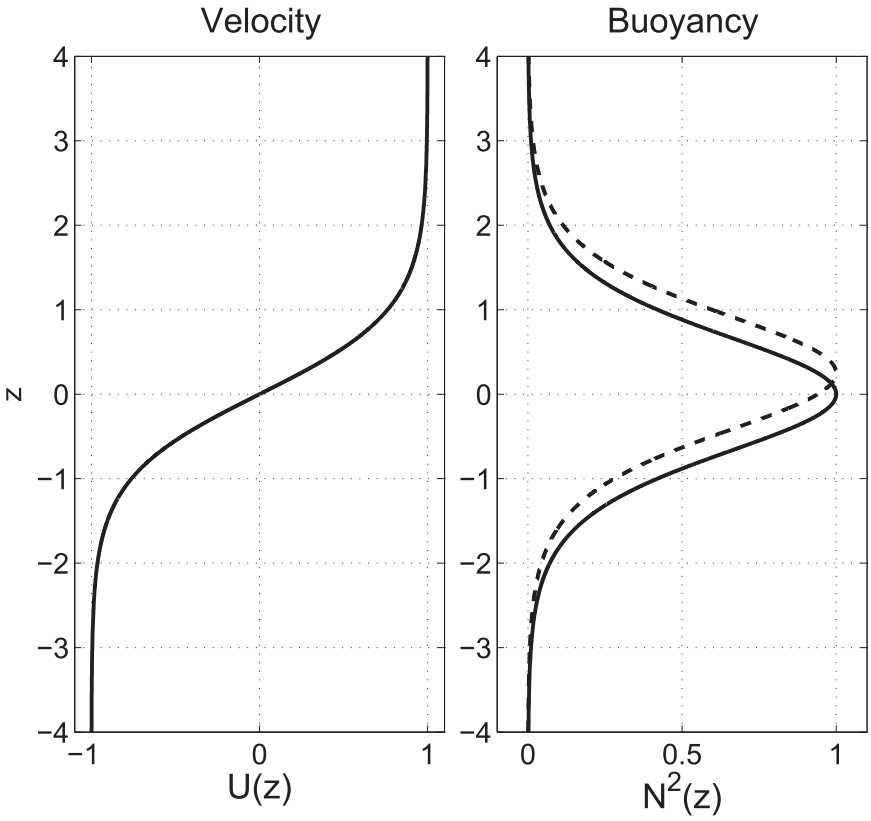

FIG. 2. (left) Mixing layer velocity and (right) buoyancy profiles. The buoyancy profile for the Hazel problem [Eq. (23), solid curve] and for the misaligned stratification and shear profiles [Eq. (24) with $d = 0.25$, dashed curve] are shown.

and right portions of the stability boundary, and critical layer approximations are necessary for accurate estimates of those eigenvalues.

It is interesting to consider how the domain height affects the stability characteristics of this problem. To that end, we imposed rigid-lid conditions and computed the locus of maximal instability in the (α, J) plane for several values of H (Fig. 4). Recall that the growth rate of an unstable mode is defined by $\omega_i = \alpha c_i$. To our knowledge, the case $H \to \infty$ is the only available value for comparison, and our results agree with those reported by Hazel (1972) to three or four significant digits. These curves, along with the stability boundary for $H \to \infty$ shown in Fig. 3, demonstrate the known phenomenon of longwave destabilization due to boundaries. We see that when $H \to \infty$ and α is near zero, instability is only possible for weak stratifications $J < \alpha(1 - \alpha)$. From the curves of maximum instability, however, it is apparent that decreasing H tends to shift the most unstable modes to longer wavelengths. In fact, for $H \approx 2.7$ longwave instability is possible even for strong stratifications with J near one-quarter.

Another interesting observation from Fig. 4 is the change in character of the curves of maximum instability for large and small H values. For $H \geq 5$, we observe that these curves are nearly vertical, with a slight rightward bend. However, as H decreases below 4, they veer sharply to the longer wavelength regime.

In Fig. 5 we plot the growth rates ω_i of the most unstable modes as a function of J and observe the expected trend toward weaker instability with increasing stratification strength. The maximal growth rates at large J values are very similar for each observed value of $H \geq 2.7$.

The longwave destabilization effect is especially pronounced when we compute the largest J value for which instability can be found at $\alpha = 0$ (Fig. 6, solid curve). Denoting these critical J values by J^*, we see from the figure that J^* initially increases as H is decreased from ∞, attaining a maximum near $H \approx 2.7$, after which J^* rapidly decreases. For $H \leq 1.2$, no unstable modes for the problem can be found. These results are in agreement with those reported by Hazel (1972), who compared the longwave stability of the shear layer to that of a two-layer fluid to explain the critical value $H = 2.7$.

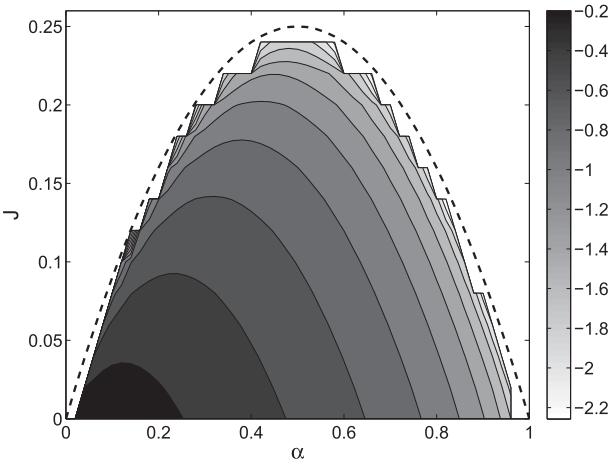

FIG. 3. A contour map of $\log_{10}(c_i)$ for the mixing layer example [Eq. (23)]. Radiation BCs were used to approximate an unbounded domain. The dashed line represents the analytical stability boundary, and no unstable modes are visible outside of the predicted unstable region. The jaggedness of the contours near the stability boundary is an artifact of the resolution in α and J used for this calculation.

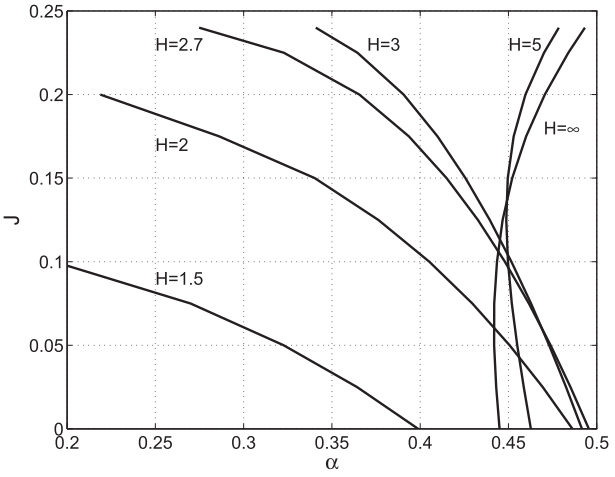

FIG. 4. The locus of maximum instability at different domain half-widths. At each value of J, a bound-constraint optimization problem was solved to determine the most unstable wavenumber α.

From a physical perspective, the destabilization of long waves by boundaries is of some importance in the geophysical setting. Even in atmospheric models with only one rigid boundary, the phenomenon is observed. Varying the proximity of a velocity inflection point to the boundary can cause substantial changes in the stability characteristics of long waves (see Lalas and Einaudi 1976 for a discussion).

c. *Asymmetric mixing layers*

We now modify the Hazel (1972) problem by investigating the effects of a misalignment of the density and velocity profiles. We consider profiles of the form

$$U(z) = \tanh(z), \quad N^2(z) = \operatorname{sech}^2(z - d), \qquad (24)$$

where the parameter d sets the offset of the stratification profile from the shear profile. A sample stratification profile with $d = 0.25$ is presented in Fig. 2 (dashed curve). As a model of mixing layers, the case $d = 0$ has been used extensively. However, given that natural flows do not possess this degree of symmetry, it is worth considering how a minor (or major) perturbation in the alignment of the stratification and shear might alter the stability characteristics of the flow. This form of asymmetry was considered by Carpenter et al. (2010) in their study concerning transitions from Kelvin–Helmholtz-type to Holmboe-type instabilities.

We note that the stability characteristics for the flow are identical for misalignments of $+d$ and $-d$. To understand this, first note that for any velocity and buoyancy profile with an eigenvalue c, the complex conjugate c^* is also an eigenvalue. Next, with $N^2(z)$ an even function about d and $U(z)$ an odd function about zero, we also see that any eigenvalue c for the offset $+d$ corresponds to an eigenvalue $-c$ at an offset of $-d$. Naturally, it follows that if c is an unstable eigenvalue for the offset $+d$, then $-c^*$ is an unstable eigenvalue for the problem with an offset of $-d$. The sign of d changes only the direction of propagation of an unstable mode, not the growth rate. This argument is valid for flows on unbounded domains and finite domains with rigid boundaries. However, on finite domains with radiating boundary conditions, the coupling of an eigenvalue c with its complex

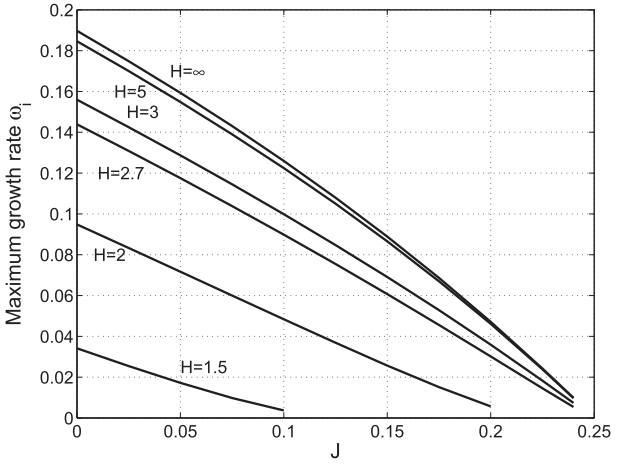

FIG. 5. The growth rate $\omega_i = \alpha c_i$ of the most unstable wave as a function of J for different domain half-widths.

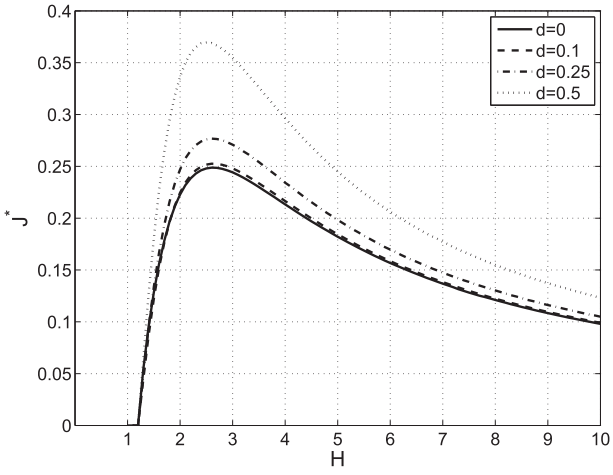

FIG. 6. Longwave destabilization as a function of the domain half-width H at various offset values d. The critical value J^* is the largest value of J for which instability can be found at $\alpha = 0$.

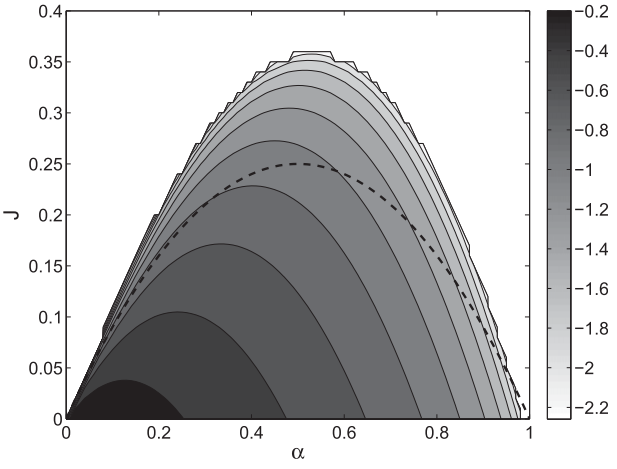

FIG. 7. Contours of $\log_{10}(c_i)$ for the asymmetric mixing layer profile with $d = 0.5$. Misalignment of the velocity and buoyancy profiles introduces unstable modes at larger values of J, and beyond the stability boundary for the aligned case $d = 0$ (dashed line).

conjugate c^* is broken (Sun et al. 1998), so the stability characteristics of flows with offsets $+d$ and $-d$ may differ.

As a rough first estimate of the effects of a misalignment ($d \neq 0$), we can use the Richardson number criterion (2) to predict that as $|d|$ increases, the flow will become susceptible to instability at larger J values. This is confirmed by the structure of the contours of $\log_{10}(c_i)$ for the case $d = 0.5$ (Fig. 7). These contours are qualitatively similar to those in the $d = 0$ case, with the largest c_i values found near the origin in the (α, J) plane, but unstable modes exist for J values outside of the $d = 0$ stability boundary.

We now return to Fig. 6 and consider the largest value of J for which longwave instability can be found as rigid-lid boundaries are moved in from infinity. Curves are displayed at offset values of $d = 0, 0.1, 0.25, 0.5$. We observe that while the critical value of $H^* \approx 2.7$ at $d = 0$ is reduced to $H^* \approx 2.5$ when $d = 0.5$, the overall shape of the curve is unchanged by the offset. The longwave destabilization effect appears to be qualitatively robust to the misalignment of the buoyancy and velocity profiles.

This example serves as a step toward justifying the use of the symmetric mixing layer as a model of real geophysical flows. Though nature will seldom offer a flow with perfect symmetry, the qualitative similarity in stability characteristics with the asymmetric model supports the choice of the symmetric model to approximate flow profiles. A much more thorough investigation of the effects of various perturbations to the flow symmetry is necessary for a detailed quantitative understanding of their qualitative implications.

d. An approximately layered flow

In Drazin and Reid (1981), a piecewise linear profile with analytical stability boundaries is presented. The problem considered there is

$$U(z) = \begin{cases} 1 & \text{if} \quad z > 1, \\ z & \text{if} \quad |z| \leq 1, \\ -1 & \text{if} \quad z < -1, \end{cases} \tag{25}$$

with

$$N^2(z) = \delta(z-1) + \delta(z+1), \tag{26}$$

where $\delta(z)$ is the Dirac-delta function.

In each of the regions $z > 1$, $|z| \leq 1$, $z < -1$, a solution to the TG equation can be easily found, and using continuity of both pressure and the vertical component of wave velocity at $z = \pm 1$, the solutions can be matched across the interfaces. The resulting equation for the phase speed is

$$4\alpha^2(1-c^2)^2 + (e^{-4\alpha}-1)c^2 - 4\alpha[J(1+c^2)+1-c^2] - (e^{-4\alpha}-1)(J+1)^2 = 0. \tag{27}$$

With some algebraic effort (for a proof see Goldstein 1931), the coefficients of this polynomial in c can be analyzed to show that the flow is unstable if and only if

$$\frac{2\alpha}{1+e^{-2\alpha}} - 1 < J < \frac{2\alpha}{1-e^{-2\alpha}} - 1. \tag{28}$$

This is a particularly interesting and counterintuitive result, suggesting Eqs. (25) and (26) are a flow for which the stratification can have a destabilizing influence. At any fixed α value, the unstratified flow is linearly stable. As J increases, though, there is a window of J values for which the flow is unstable. For J above this window, the flow is again stabilized. A detailed discussion of this profile and others where stratification has a destabilizing influence is presented in Howard and Maslowe (1973), and they describe vorticity generated by the nonhomogeneity of the fluid as the underlying physical mechanism at work.

Directly computing the unstable modes of Eqs. (25) and (26) with TGsolver is not possible because of the presence of the δ functions and discontinuities in the derivatives of U. However, we can study a smoothed version of the problem numerically and look for the destabilizing effect of stratification. With that goal, we consider

$$U(z) = [\tanh(z^n)]^{1/n},$$
$$N^2(z) = \frac{1}{2\beta}\left[\operatorname{sech}^2\left(\frac{z-1}{\beta}\right) + \operatorname{sech}^2\left(\frac{z+1}{\beta}\right)\right], \quad (29)$$

where n is a positive integer and β is a width parameter.

Contours of the $\log_{10}(c_i)$ for this smoothed profile with $n = 5$ and $\beta = 0.05$ are presented in Fig. 8 (solid lines). The phase speeds of the idealized problem [Eqs. (25) and (26)] were computed as solutions to Eq. (27) and included in the figure as dashed lines, also logarithmically scaled. The analytical stability boundaries [Eq. (28)] are displayed as thin solid lines. We see that the unstable modes of the smoothed problem are confined to the same region as those of the idealized problem. The eigenvalues for the two problems are also very similar, as is evident from the minor differences in the contour lines. The c_i values obtained via TGsolver agree with those of the smoothed problem to within a relative error of roughly 10^{-3} within the core of the unstable region.

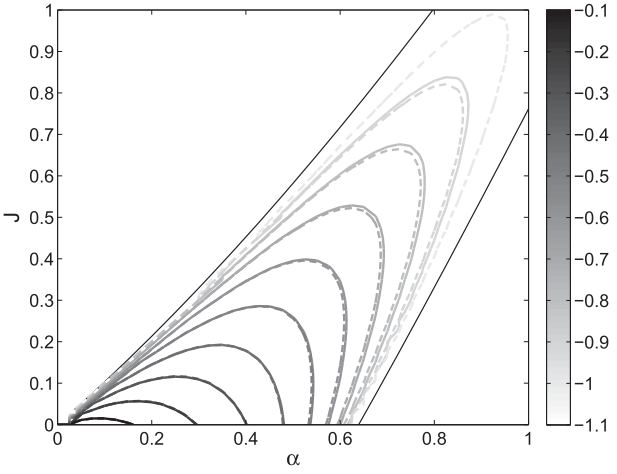

FIG. 8. Contours of $\log_{10}(c_i)$ for the smoothed multilayer problem [Eq. (29); solid lines] and its idealized counterpart (dashed lines). Stability boundaries for the idealized problem are marked with thin black lines. At fixed α the stratification is observed to destabilize the flow through a band of J values. The eigenvalues of the idealized and smooth profiles are in good agreement within the core of the unstable region, with larger differences evident near the boundaries.

4. Discussion

The examples presented above provide a small sample of the types of problems that can be explored with TGsolver. The ability to compute unstable modes for given flow profiles will enable researchers to pursue many interesting questions about flow stability. It must be noted, however, that TGsolver does have limitations and will perform best under certain conditions, as we now discuss.

Currently, TGsolver is capable of handling at most one critical layer in a stability calculation. This suggests that TGsolver is ideal for monotonic velocity profiles, so that multiple approximations are not required. Our approach of solving the minimization problem [Eq. (7)] does allow us to circumvent this limitation to some extent. By simply setting the minimum imaginary phase speed cutoff δ to be appropriately large, the problems associated with critical layers can be completely removed. In fact, we recommend that for any calculations on a new flow profile, a large value of δ be used initially. This will enable a relatively fast initial exploration of the parameter space. For many purposes, such as where only the largest c_i values are of interest, such an analysis should provide adequate results.

Another issue that TGsolver cannot handle is the presence of critical layers at, or very near, a domain boundary. Studies on flows where this is possible can still be conducted; our use of a constrained minimization approach allows us to restrain iterates away from the boundaries. Numerically, this is implemented by simply adding bound constraints on c_r.

The performance of TGsolver is affected by the number of points used in the initial discretization of Howard's semicircle. Increasing the density of points within the semicircle generally improves the method's ability to detect unstable modes (as better initial guesses for the optimization procedure will be available). However, this improvement must be balanced against the additional computational time that is required.

TGsolver's performance for a particular problem will also depend on the choice of the critical layer slope

threshold. The value used for the examples included here led to robust results for the problems considered, but there is no guarantee that it will be suitable for other flow profiles. The value is left as a user-defined parameter. It is important to note that, by increasing the threshold value, fewer critical layer approximations will be used, and in some cases this will lead to spurious solutions. Some experimentation may be required for best results. Additional experiments comparing Legendre, finite-difference, and other differentiation techniques with the Chebyshev approach may also prove fruitful.

5. Conclusions

We have presented a numerical method for finding unstable modes of the Taylor–Goldstein equation. Our approach uses a shooting method and reduces the eigenvalue problem to a constrained optimization problem (7). The description presented here is implemented in a set of MATLAB programs known as TGsolver, and can be downloaded (web.uvic.ca/~monahana/TGsolver/TGsolver.html). Updates to the program will also be available from this site.

The purpose of TGsolver is to provide a useful tool for researchers to study the stability characteristics of inviscid, stratified parallel shear flows. The singular nature of the TG equation makes it difficult to build a robust solution for all flows of interest, and some of the limitations of our approach are highlighted in section 4. Our constrained optimization approach does allow us to overcome some of the limitations when only large c_i values are of interest. Where possible, TGsolver calculations were compared with existing results and were found to be in good agreement.

In future work, we will extend TGsolver functionality to handle multiple critical layers. We shall also apply the approach to the analysis of the stability of observed geophysical flows.

Acknowledgments. We thank the NSERC CREATE Program in Interdisciplinary Climate Science for funding this research. A. M. also acknowledges support from the NSERC Discovery Grants program. We would also like to thank Norm McFarlane for the many useful discussions.

APPENDIX A

Implementation of TGsolver in MATLAB

TGsolver is implemented in the MATLAB programming language, and the majority of the necessary support functions are custom made and included with the code. The exceptions are presented in Table A1.

TABLE A1. Special MATLAB functions required by TGsolver.

Function	Purpose	Source
fmincon	Constrained optimization routine	Optimization Toolbox
kmeans	*k*-means clustering	Statistics Toolbox
cheb	Chebyshev differentiation matrices	Trefethen (2000)

Initial experiments were conducted using Muller interpolation (a generalization of the secant method to root finding in the complex plane), but the constrained optimization approach was adopted, as it allows for control over the singularity of the equation. The MATLAB function *fmincon* is set to use the interior point algorithm. Essentially, this algorithm works by attempting Newton steps to minimize a merit function. The merit function incorporates equality and inequality constraint satisfaction in a manner that steers the solution toward feasibility. A detailed description of the method can be found on MathWorks's documentation page for constrained nonlinear optimization algorithms.

The *k*-means algorithm is a classic data clustering technique where data points are assigned to a preset number of clusters. In *k*-means, data points are assigned to the nearest cluster based on the Euclidean distance to the cluster centers. The process is by necessity iterative, as the assignment of points alters the locations of the cluster centers. The clustering of partially converged iterates is done to reduce run time for TGsolver. Starting from each grid point within Howard's semicircle and allowing the constrained optimization solver to execute a large number of iterations is excessively time consuming. Experience dictates that after just a few iterations, the poorly converged iterates can be discarded. Using *k*-means enables us to lump together many of the remaining iterates and reduce the number of times that the solver finds the same solution.

APPENDIX B

Expansions for Critical Layers

Here we present Frobenius series expansions that capture the behavior of eigenfunctions near a critical point for the TG equation. Two linearly independent series solutions are required for matching boundary conditions across a critical layer. Within TGsolver we typically use just the leading-order component of each series approximation, but the number of terms used in each approximation can be modified.

Throughout this analysis we assume that $U'(z_c) \neq 0$. The Rayleigh problem is treated separately, as the solutions are qualitatively different. The analysis here closely follows the framework presented by Bender and Orszag (1999).

a. General notation

We analyze the behavior of an eigenfunction about a critical point z_c, denoting $N_c = N(z_c)$, $U_c = U(z_c)$, $U_c' = U'(z_c)$, and $U_c'' = U''(z_c)$. For this analysis, we assume that $N^2(z)$ and $U(z)$ are C^∞ functions. We define $z_0 = z_c + ic_i/U_c'$ and analyze

$$\phi''(z) + \left[\frac{q_0 + q_1(z - z_0) + q_2(z - z_0)^2}{(z - z_0)^2}\right]\phi(z) = 0 \quad \text{(B1)}$$

about z_0. We note that, provided $U_c' \neq 0$, z_0 is a regular singular point. We also note that by writing the TG equation in this form, we have truncated the Taylor expansions for $N^2(z)$ and $U(z)$, so the series solutions we obtain will only provide exact representations when $N(z)$ is constant and $U(z)$ is linear.

We seek Frobenius series solutions of the form

$$\phi(z) = \sum_{n=0}^{\infty} a_n (z - z_0)^{n+r}. \quad \text{(B2)}$$

The coefficients satisfy the recurrence relation

$$[(n + r)(n + r - 1) + q_0]a_n + q_1 a_{n-1} + q_2 a_{n-2} = 0. \quad \text{(B3)}$$

b. Expansions for the TG equation

In the context of the TG equation, $q_0 = JN_c^2/U_c'^2 \neq 0$ is the local Richardson number, $q_1 = -U_c''/U_c'$, and $q_2 = -\alpha^2$. The indicial equation is $r^2 - r + q_0 = 0$, yielding $r = 1/2 \pm \sqrt{1/4 - q_0}$. By convention we label the roots so that $r_1 > r_2$ when $q_0 < 1/4$.

If $q_0 \neq 1/4$, then two linearly independent solutions of the form (B2) with $r = r_1$, r_2 are available, and we are finished. We must also consider the degenerate case $q_0 = 1/4$, for which one solution of the form (B2) is available with $r = 1/2$. To find the second solution, we let L denote the TG differential operator and define $\xi(z, r)$ as a series of the form (B2), with r-dependent coefficients satisfying (B3). Then

$$L\xi(z, r) = z_0(r - 1/2)^2(z - z_0)^{r-2}. \quad \text{(B4)}$$

Differentiating both sides with respect to r reveals $L\partial_r \xi(z, r)|_{r=1/2} = 0$, suggesting $\partial_r \xi(z, r)|_{r=1/2}$ is the second linearly independent solution. To evaluate $\partial_r \xi(z, r)$, we first write $(z - z_0)^{n+r} = \exp[(n + r)\log(z - z_0)]$, and recalling that a_n is a function of r, we find the second linearly independent solution is

$$\phi_2(z) = \log(z - z_0)\phi_1(z) + \sum_{n=1}^{\infty} a_n'(z - z_0)^{n+1/2}, \quad \text{(B5)}$$

where $a_n' = (da_n/dr)_{r=1/2}$. We fix $a_0 = 1$ for $\phi_1(z)$ and $\phi_2(z)$.

c. Expansions for the Rayleigh equation

Now we fix $q_0 = 0$ in (B1), and again seek a Frobenius series of the form (B2). The indicial equation becomes $r(r - 1) = 0$, and we label the two roots $r_1 = 1$, $r_2 = 0$. Coefficients satisfy the recurrence (B3) with $q_0 = 0$. The Frobenius solution (B2) is valid for $r = r_1$, and we label it $\phi_1(z)$ with $a_0 = 1$. However, since $r_1 - r_0 = 1$ is a positive integer, a more elaborate analysis is needed to find the second solution.

To find $\phi_2(z)$, we consider $\xi(z, r) = \sum_{n=0}^{\infty} b_n(z - z_0)^{n+r}$, where each b_n depends on r and satisfies (B3) with $b_0 = 1$. Denoting the Rayleigh differential operator by L, we have

$$L\xi(z, r) = b_0 r(r - 1)(z - z_0)^{r-2}. \quad \text{(B6)}$$

Differentiating with respect to r, and evaluating at $r = 1$, we find that:

$$L\left.\frac{\partial \xi(z, r)}{\partial r}\right|_{r=r_1} = b_0(z - z_0)^{-1}. \quad \text{(B7)}$$

But $b_n|_{r=1} = a_n$, as they satisfy the same recurrence with the same initial condition, so we find:

$$\left.\frac{\partial \xi(z, r)}{\partial r}\right|_{r=r_1} = \log(z - z_0)\phi_1(z) + \sum_{n=1}^{\infty} b_n'(z - z_0)^{n+1}, \quad \text{(B8)}$$

where $b_n' = (db_n/dr)_{r=r_1}$ and $b_0' = 0$. We require a particular solution $\eta(z)$ such that $L\eta(z) = b_0/(z - z_0)$. We expand the particular solution in the series form $\eta(z) = b_0/q_1 + \beta\phi_1(z)$, where β is a constant. Our second solution, $\phi_2(z)$ is then given by $\phi_2(z) = \eta(z) - [\partial_r \xi(z, r)]_{r=1}$; that is,

$$\phi_2(z) = \frac{1}{q_1} - \left[\log(z - z_0)\phi_1(z) + \sum_{n=1}^{\infty} b_n'(z - z_0)^{n+1}\right]. \quad \text{(B9)}$$

Note that we dropped the contribution $\beta\phi_1(z)$ from this solution. This is possible because our purpose is to construct two linearly independent functions from which

any solution about the critical point can be represented. These solutions agree with the leading-order components given by Maslowe (1986).

d. Estimating critical layer width

Our analysis thus far has been restricted to finding series approximations for (B1), which is itself an approximation of the TG equation. We now argue that when $|z - z_c|$ is sufficiently small, the idealized Eq. (B1) does adequately represent the behavior of eigenfunction solutions near critical layers, and it does use our analysis to heuristically determine an appropriate width of the critical layer.

First, we note that as $z \to z_c$, we have

$$\begin{aligned} N^2(z) &= N_c^2 + \mathcal{O}(z - z_c), \\ U''(z) &= U_c'' + \mathcal{O}(z - z_c), \end{aligned} \tag{B10}$$

where we use big-$\mathcal{O}$ notation to estimate the order of the terms. Similarly, we can expand

$$\frac{1}{(U-c)^2} = \frac{1}{U_c'^2(z-z_0)^2} \frac{1}{\left\{1 + \dfrac{U_c''}{2U_c'}\dfrac{(z-z_c)^2}{z-z_0} + \mathcal{O}\left[\dfrac{(z-z_c)^3}{z-z_0}\right]\right\}^2}. \tag{B11}$$

Now, provided $|(U_c''/2U_c')([z-z_c)^2/z-z_0]| \ll 1$, we can use the identity $1/(1+x)^2 = 1 - 2x + 3x^2 \ldots$ to expand

$$\begin{aligned} &\frac{1}{\left\{1 + \dfrac{U_c''}{2U_c'}\dfrac{(z-z_c)^2}{z-z_0} + \mathcal{O}\left[\dfrac{(z-z_c)^3}{z-z_0}\right]\right\}^2} \\ &\quad = 1 - \frac{U_c''}{U_c'}\frac{(z-z_c)^2}{z-z_0} + \mathcal{O}\left[\frac{(z-z_c)^3}{z-z_0}\right]. \end{aligned} \tag{B12}$$

Next, we observe that, provided $|z - z_c| < |c_i/U_c'|$, for z near z_c we can write

$$\begin{aligned} \frac{z-z_c}{z-z_0} &= \frac{z-z_c}{ic_i/U_c'} \frac{1}{1 + \dfrac{z-z_c}{ic_i/U_c'}} \\ &= \frac{z-z_c}{ic_i/U_c'}\left\{1 - \frac{z-z_c}{ic_i/U_c'} + \mathcal{O}\left[\left(\frac{z-z_c}{c_i/U_c'}\right)^2\right]\right\}, \\ &= \frac{z-z_c}{ic_i/U_c'} + \mathcal{O}\left[\left(\frac{z-z_c}{c_i/U_c'}\right)^2\right], \end{aligned} \tag{B13}$$

where a geometric series has been used to expand the rightmost term in the first line.

Combining these arguments, we see that in the vicinity of a critical layer, the TG equation becomes

$$\phi''(z) + \left[\frac{JN_c^2/U_c'^2 - U_c''/U_c'(z-z_0) - \alpha^2(z-z_0)^2 + \mathcal{O}(z-z_c)}{(z-z_0)^2}\right]\phi(z) = 0. \tag{B14}$$

This justifies our analysis of (B1), at least to leading order. Our arguments suggest that the critical layer approximations will be appropriate in an interval satisfying

$$|z - z_c| \ll \min\left\{\sqrt{\left|\frac{2c_i}{U_c''}\right|}, \left|\frac{c_i}{U_c'}\right|\right\}. \tag{B15}$$

Within TGsolver we typically select a critical layer half-width of $\Delta_{cl} = \epsilon c_i/U_c'$ with $\epsilon = 0.01$. Experience has shown that a larger multiplier tends to decrease the accuracy in the solution, when comparing with known results. For instance, using the growth rate of 0.0472 as reported at $J = 0.2$ in Fig. 1 of Hazel's (1972) paper, we find that our relative error in the estimate of the growth rate behaves like $\log(\text{Relative error}) \approx \log(\epsilon)$; that is, an order-of-magnitude increase in ϵ results in an order-of-magnitude increase in the relative error of the growth rate.

Taking ϵ too small can also have a negative impact, as for small c_i values the slope of the solution near the critical layer will grow dramatically. Experience has shown that with ϵ too small, or without using a critical layer at all, unstable modes may be found in regions of stability purely due to numerical error. The choice of $\epsilon = 0.01$ may not work for all problems, especially where critical layers lie very close to boundaries, and some experimentation may be required.

REFERENCES

Ascher, U. M., R. M. Mattheij, and R. D. Russell, 1988: *Numerical Solution of Boundary Value Problems for Ordinary Differential Equations.* Prentice-Hall, 619 pp.

Bender, C. M., and S. A. Orszag, 1999: *Advanced Mathematical Methods for Scientists and Engineers: Asymptotic Methods and Perturbation Theory.* Springer-Verlag, 593 pp.

Carpenter, J. R., N. J. Balmforth, and G. A. Lawrence, 2010: Identifying unstable modes in stratified shear layers. *Phys. Fluids,* **22,** 054104, doi:10.1063/1.3379845.

De Baas, A. F., and A. G. M. Driedonks, 1985: Internal gravity waves in a stably stratified boundary layer. *Bound.-Layer Meteor.,* **31,** 303–323, doi:10.1007/BF00120898.

Drazin, P. G., and W. H. Reid, 1981: *Hydrodynamic Stability.* Cambridge University Press, 525 pp.

Goldstein, S., 1931: On the stability of superposed streams of fluids of different densities. *Proc. Roy. Soc. London,* **132A,** 524–548, doi:10.1098/rspa.1931.0116.

Hazel, P., 1972: Numerical studies of the stability of inviscid stratified shear flows. *J. Fluid Mech.,* **51,** 39–61, doi:10.1017/S0022112072001065.

Howard, L. N., and S. A. Maslowe, 1973: Stability of stratified shear flows. *Bound.-Layer Meteor.,* **4,** 511–523, doi:10.1007/BF02265252.

Kundu, P. K., and I. M. Cohen, 2004: *Fluid Mechanics.* 3rd ed. Elsevier Academic Press, 759 pp.

Lalas, D. P., and F. Einaudi, 1976: On the characteristics of gravity waves generated by atmospheric shear layers. *J. Atmos. Sci.,* **33,** 1248–1259, doi:10.1175/1520-0469(1976)033<1248:OTCOGW>2.0.CO;2.

Maslowe, S. A., 1986: Critical layers in shear flows. *Annu. Rev. Fluid Mech.,* **18,** 405–432, doi:10.1146/annurev.fl.18.010186.002201.

Mastrantonio, G., F. Einaudi, D. Fua, and D. P. Lalas, 1976: Generation of gravity waves by jet streams in the atmosphere. *J. Atmos. Sci.,* **33,** 1730–1738, doi:10.1175/1520-0469(1976)033<1730:GOGWBJ>2.0.CO;2.

Michalke, A., 1964: On the inviscid instability of the hyperbolic-tangent velocity profile. *J. Fluid Mech.,* **19,** 543–556, doi:10.1017/S0022112064000908.

Mobbs, S. D., and M. S. Darby, 1989: A general method for the linear stability analysis of stratified shear flows. *Quart. J. Roy. Meteor. Soc.,* **115,** 915–939, doi:10.1002/qj.49711548808.

Smyth, W. D., J. N. Moum, and J. D. Nash, 2011: Narrowband oscillations in the upper equatorial ocean. Part II: Properties of shear instabilities. *J. Phys. Oceanogr.,* **41,** 412–428, doi:10.1175/2010JPO4451.1.

Sun, C., W. D. Smyth, and J. N. Moum, 1998: Dynamic instability of stratified shear flow in the upper equatorial Pacific. *J. Geophys. Res.,* **103,** 10 323–10 337, doi:10.1029/98JC00191.

Taylor, G. I., 1931: Effect of variation in density on the stability of superposed streams of fluid. *Proc. Roy. Soc. London,* **132A,** 499–523, doi:10.1098/rspa.1931.0115.

Tedford, E. W., J. R. Carpenter, R. Pawlowicz, R. Pieters, and G. A. Lawrence, 2009: Observation and analysis of shear instability in the Fraser River estuary. *J. Geophys. Res.,* **114,** C11006, doi:10.1029/2009JC005313.

Trefethen, L. N., 2000: *Spectral Methods in MATLAB.* Software, Environments, and Tools, Vol. 10, SIAM, 165 pp.